# Power Converter Topologies for Wind Energy Conversion Systems: Integrated Modeling, Control Strategy and Performance Simulation

R. Melício[a], V.M.F. Mendes[b], J.P.S. Catalão[a,*]

[a] *Department of Electromechanical Engineering, University of Beira Interior, R. Fonte do Lameiro, 6201-001 Covilha, Portugal*
[b] *Department of Electrical Engineering and Automation, Instituto Superior de Engenharia de Lisboa, R. Conselheiro Emídio Navarro, 1950-062 Lisbon, Portugal*

Received 24 October 2008; received in revised form 13 February 2010

**Abstract**

This paper presents new integrated model for variable-speed wind energy conversion systems, considering a more accurate dynamic of the wind turbine, rotor, generator, power converter and filter. Pulse width modulation by space vector modulation associated with sliding mode is used for controlling the power converters. Also, power factor control is introduced at the output of the power converters. Comprehensive performance simulation studies are carried out with matrix, two-level and multilevel power converter topologies in order to adequately assert the system performance. Conclusions are duly drawn.


*Keywords:* Modeling; Power system stability; Wind power generation

## 1. Introduction

Electricity restructuring has offered us additional flexibility at both levels of generation and consumption. Also, since restructuring has strike the power system sector, developments in distributed power generation systems (DPGSs) opened new perspectives for electric companies [1]. DPGSs include, for instances, wind turbines, wave generators, photovoltaic generators, small hydro, and fuel cells. A detailed description of the hardware structure for several DPGSs is given in [2]. An overview of control and grid synchronization for DPGSs is given in [3]. Among DPGSs, the development of wind power generation in recent years is significant, even envisaged as competing with the traditional fossil-fuelled thermal power generation in the near future due to its environmental value.

* Corresponding author. Tel.: +351 275 329914; fax: +351 275 329972.
*E-mail address:* catalao@ubi.pt (J.P.S. Catalão).

Environmental concerns are becoming increasingly relevant for electric companies as regulations on pollutants become more severe, and customer awareness of environmental impacts increases. It is now recognized that the greenhouse effect can be slowed down only if $CO_2$ emissions are reduced drastically [4]. Recently, the European Commission put forward a set of proposals to create a new Energy Policy for Europe, cutting its own $CO_2$ emissions by at least 20% by 2020 and 50% until 2050, increasing the share of renewable energy sources in the overall generation mix. Hence, it is expected that wind energy will turn out to be an important part of the future Energy Policy for Europe.

In Portugal, the total installed renewable energy capacity reached 8908 MW in October 2009, of which wind power capacity is responsible for 3455 MW, and continues growing. An overview of the Portuguese technical approaches and methodologies followed in order to plan and accommodate the ambitious wind power goals to 2010/2013, preserving the overall quality of the power system, is given in [5].

The increasing share of wind in power generation will change considerably the dynamic behavior of the power system [6], and may lead to a reduction of power system frequency regulation capabilities [7]. In addition, network operators have to ensure that consumer power quality is not compromised [8]. Hence, new technical challenges emerge due to the increased wind power penetration, dynamic stability and power quality, implying research of more realistic physical models for wind energy conversion systems (WECSs) [9-11].

Power-electronic converters have been developed for integrating wind power with the electric grid. The use of power-electronic converters allows for variable-speed operation of the wind turbine, and enhanced power extraction. In variable-speed operation, a control method designed to extract maximum power from the wind turbine and provide constant grid voltage and frequency is required [12]. Variable-speed WECSs offer the following advantages: mechanical stress is reduced, torque oscillations are not transmitted to the grid, and below rated wind speed the rotor speed is controlled to achieve maximum aerodynamic efficiency.

The variable-speed WECSs are implemented with either doubly fed induction generators (DFIGs) [13] or full-power converters [14]. In a variable-speed WECS with full-power converter, the generator is completely decoupled from the grid [8].

In recent years, the rotor size of new wind turbine designs has been significantly increased in order to extract more power from wind [15] and increase performance of WECSs. The future tendency for large WECSs is to reduce the number of mechanical components, to decrease weight and costs associated with the construction. Eliminating the need for a gearbox will eliminate a significant component, which is responsible for mechanical energy losses and unpleasant audible sounds.

Reference [16] states that variable-speed WECSs with permanent magnet synchronous generator (PMSG) are a promising concept for large offshore wind farms. For offshore application, reliability is an important factor for economic efficiency since maintenance and repair are extremely expensive and not guaranteed at any time due to difficult access to the offshore wind turbines in bad weather conditions [17]. Reference [12] states that PMSG is generally favored in newer smaller scale turbine design, since it allows for higher efficiency and smaller wind turbine blade diameter. Reference [18] points the advantage of full-power converter WECSs: control of active and reactive power output. Reference [19] presents a dynamic model for variable-speed WECSs, equipped with a variable pitch wind turbine, a synchronous electric generator, and a full-power converter.

In this paper, a variable-speed wind turbine is considered with PMSG and three different power converter topologies: matrix, two-level and multilevel.

The matrix converter is capable of a direct conversion of the generator variable AC frequency into the grid constant AC frequency. Thus, it is an AC-AC converter. A technology review of matrix converters can be seen in [20]. Two distinct advantages arise from this topology, the converter requires no bulky energy storage or DC-link, and control is performed on just one converter [12]. Also, the converter is smaller, lighter and more reliable than conventional converters. Because of these characteristics matrix converters are a good alternative for the variable-speed operation of WECSs [21]. One of the major drawbacks of a matrix converter is that eighteen total switches are required, causing an increase in converter cost. Also, industrial wide use of matrix converter is still limited due to certain undesirable characteristics: sensitivity to distortion in input power supply due to the lack of reactive component in the power circuit; and sensitivity to the rapidly fluctuating input voltage frequency when used in WECSs [22].

Multilevel converters are AC-DC-AC converters, well suited for medium and high-power applications [23] due to their ability to meet the increasing demand of power ratings and power quality associated with reduced harmonic distortion, lower electromagnetic interference, and higher efficiencies when compared with the conventional two-level topology [24,25]. A survey of topologies, controls, and applications for multilevel inverters can be seen in [26].

The increasing number of voltage levels lead to the production of high power quality waveforms [27], causing the total harmonic distortion (THD) to be lower. Multilevel converters, and specifically three-level converters, are a good tradeoff solution between performance and cost in high-power systems [28]. Multilevel converters are, however, limited by the following drawbacks: voltage unbalances, high component count, and increased control complexity [24]. A critical issue in three-level converters is the design of the DC-link capacitors. Thus, special attention should be paid to the unbalance in the voltage of the capacitors for the three-level converters, which may produce a malfunction of the control. One possible design of the DC-link is given in [29]. Reference [30] proposes a control methodology that achieves the regulation of torsional dynamics and the DC-link capacitor voltage without involving the grid-side converter controls, eliminating the influence of those dynamics on the grid.

Several papers have been issued on matrix, two-level or multilevel power converters, but mainly using simplified models to describe the WECS or the control strategies themselves. However, the increased wind power penetration, as nowadays occurs for instance in Portugal, requires new models and system operation tools.

As a new contribution to earlier studies, a more realistic modeling of WECS with different power converter topologies is presented in this study, combined with a complex control strategy, and comprehensive performance simulation studies are carried out in order to adequately assert the system performance.

This paper is organized as follows. Section II presents the integrated modeling of the WECS with different power converter topologies: matrix, two-level and multilevel. Section III presents the control strategy: pulse width modulation (PWM) by space vector modulation (SVM) associated with sliding mode is used for controlling the converters, and power factor control is introduced at the output of the converters. Section IV presents the design of the power coefficient as a function of the wind speed. Section V presents the case study and the simulation results. Finally, concluding remarks are given in Section VI.

## 2. Integrated modeling

### *2.1 Wind turbine and mechanical drive train*

The mechanical power of the wind turbine is given by:

$$P_t = \frac{1}{2}\rho A u^3 c_p \tag{1}$$

where $P_t$ is the mechanical power of the wind turbine, $\rho$ is the air density, $A$ is the area covered by the rotor blades, $u$ is the wind speed upstream of the rotor, and $c_p$ is the power coefficient.

The power coefficient $c_p$ is a function of the pitch angle $\theta$ of rotor blades and of the tip speed ratio λ, which is the ratio between blade tip speed and wind speed upstream of the rotor. The computation of the power coefficient requires the use of blade element theory and the knowledge of blade geometry. These complex issues are normally empirical considered. In this paper, the numerical approximation developed in [31] is followed, where the power coefficient is given by:

$$c_p = 0.73\left(\frac{151}{\lambda_i} - 0.58\theta - 0.002\theta^{2.14} - 13.2\right)e^{-\frac{18.4}{\lambda_i}} \tag{2}$$

$$\lambda_i = \frac{1}{\frac{1}{(\lambda - 0.02\theta)} - \frac{0.003}{(\theta^3 + 1)}} \tag{3}$$

The mechanical power is given by substituting (2) and (3) into (1). From (2), the global maximum for the power coefficient is at null pitch angle, and it is equal to:

$$c_{p\max} = 0.4412 \tag{4}$$

corresponding to an optimal tip speed ratio at null pitch angle, given by:

$$\lambda_{opt} = 7.057 \tag{5}$$

A blade active pitch angle controller must be included in a variable-speed WECS [18], employing pitch control when reducing the angle of attack: increasing the blade pitch angle reduces the capture of wind energy. Fig. 1 shows the power coefficient as a function of the tip speed ratio, parameterized in function of the pitch angle.

"See Fig. 1 at the end of the manuscript".

An accurate way to model a mechanical drive train of a WECS is to model the rotor as a number of equivalent discrete masses connected together by springs and dampers. When applications are limited to the impact of wind fluctuations, it is usually sufficient to consider the mechanical drive train as a single-mass shaft model because shaft oscillations of the WECS are not reflected to the grid due to the fast active power control. However, when the system response to heavy disturbances is analyzed, the rotor must be approximated by at least a two-mass model [32]. One mass represents the wind turbine moment of inertia, and the other mass represents the generator moment of inertia. The equations for modeling the mechanical drive train are given by:

$$\frac{d\omega_t}{dt} = \frac{1}{J_t}(T_t - T_{dt} - T_{at} - T_{ts}) \tag{6}$$

$$\frac{d\omega_g}{dt} = \frac{1}{J_g}(T_{ts} - T_{dg} - T_{ag} - T_g) \tag{7}$$

where $\omega_t$ is the rotor angular speed at the wind turbine, $J_t$ is the moment of inertia for the rotor of the wind turbine, $T_t$ is the mechanical torque, $T_{dt}$ is the resistant torque in the wind turbine bearing, $T_{at}$ is the resistant torque in the hub and blades due to the viscosity of the airflow, $T_{ts}$ is the torque of the torsional stiffness, $\omega_g$ is the rotor angular speed at the generator, $J_g$ is the moment of inertia for the rotor of the generator, $T_{dg}$ is the resistant torque in the generator bearing, $T_{ag}$ is the resistant torque due to the viscosity of the airflow in the generator, and $T_g$ is the electric torque.

*2.2 Generator*

The equations for modeling a PMSG can be found in the literature [33]. Using the motor machine convention, the equations are given by:

$$\frac{di_d}{dt} = \frac{1}{L_d}[u_d + p\omega_g L_q i_q - R_d i_d] \tag{8}$$

$$\frac{di_q}{dt} = \frac{1}{L_q}[u_q - p\omega_g (L_d i_d + M i_f) - R_q i_q] \tag{9}$$

where $i_f$ is the equivalent rotor current, $M$ is the mutual inductance, $p$ is the number of pairs of poles; and where in $dq$ axes, $i_d$ and $i_q$ are the stator currents, $L_d$ and $L_q$ are the stator inductances, $R_d$ and $R_q$ are the stator resistances, $u_d$ and $u_q$ are the stator voltages.

The electrical power $P_g$ is given by:

$$P_g = \begin{bmatrix} u_d & u_q & u_f \end{bmatrix} \begin{bmatrix} i_d & i_q & i_f \end{bmatrix}^T \tag{10}$$

In order to avoid demagnetization of permanent magnet in the PMSG, a null stator current $i_d = 0$ is usually imposed [34]. The output power $P$ and $Q$ injected in the grid in $\alpha\beta$ axes [35] is given by:

$$\begin{bmatrix} P \\ Q \end{bmatrix} = \begin{bmatrix} u_\alpha & u_\beta \\ -u_\beta & u_\alpha \end{bmatrix} \begin{bmatrix} i_\alpha \\ i_\beta \end{bmatrix} \tag{11}$$

where in $\alpha\beta$ axes, $i_\alpha$ and $i_\beta$ are the phase currents, $u_\alpha$ and $u_\beta$ are the phase voltages.

*2.3 Matrix converter*

The matrix converter is an AC-AC converter, with nine bidirectional commanded insulated gate bipolar transistors (IGBTs) $S_{ij}$. It is connected between the PMSG and a second order filter, which in turn is connected to an electric network. The second order filter inductive component avoids the interruption of the output currents. A switching strategy can be chosen so that the output voltages have nearly sinusoidal waveforms at the desired frequency, magnitude and phase angle, and the input currents are nearly sinusoidal at the desired displacement power factor [36]. A three-phase active symmetrical circuit in series models the electric network.

The configuration of the simulated WECS with matrix converter is shown in Fig. 2.

"See Fig. 2 at the end of the manuscript".

For the matrix converter modeling it is assumed that: 1) the diodes are ideal: in conduction it is null the voltage between its terminals, and in blockade it is null the current that passes through it; 2) the elements of the command matrix of the converter are bidirectional switches in voltage and current; 3) the command variables $S_{ij}$ for each $i$ has for one $j$ the value one, i.e., only one switch is in conduction in order to achieve continuity in the current in each phase; 4) the command variables $S_{ij}$ for each $j$ has for one $i$ the value one, i.e., only one switch is in conduction in order to achieve continuity in the voltage between the phases.

The IGBTs commands $S_{ij}$ are given in function of the on and off states as follows:

$$S_{ij} = \begin{cases} 1, \ (\text{on}) \\ 0, (\text{off}) \end{cases} \qquad i, j \in \{1, 2, 3\} \tag{12}$$

The assumptions in 3) and 4) are respectively given by:

$$\sum_{j=1}^{3} S_{ij} = 1 \qquad i \in \{1, 2, 3\} \tag{13}$$

$$\sum_{i=1}^{3} S_{ij} = 1 \qquad j \in \{1, 2, 3\} \tag{14}$$

The vector of output phase voltages is related to the vector of input phase voltages through the command matrix [10], as follows:

$$\begin{bmatrix} v_A \\ v_B \\ v_C \end{bmatrix} = \begin{bmatrix} S_{11} & S_{12} & S_{13} \\ S_{21} & S_{22} & S_{23} \\ S_{31} & S_{32} & S_{33} \end{bmatrix} \begin{bmatrix} v_a \\ v_b \\ v_c \end{bmatrix} = [S] \begin{bmatrix} v_a \\ v_b \\ v_c \end{bmatrix} \tag{15}$$

The vector of input phase currents is related to the vector of output phase currents through the command matrix [10], as follows:

$$[i_a \quad i_b \quad i_c]^T = [S]^T [i_A \quad i_B \quad i_C]^T \tag{16}$$

Hence, the matrix converter is modeled by (12) to (16).

*2.4 Two-level converter*

The two-level converter is an AC-DC-AC converter, with six unidirectional commanded IGBTs $S_{ik}$ used as a rectifier, and with the same number of unidirectional commanded IGBTs used as an inverter. The rectifier is connected between the PMSG and a capacitor bank. The inverter is connected between this capacitor bank and a first order filter, which in turn is connected to an electric network. The groups of two IGBTs linked to the same phase constitute a leg $k$ of the converter. A three-phase active symmetrical circuit in series models the electric network.

The configuration of the simulated WECS with two-level converter is shown in Fig. 3.

"See Fig. 3 at the end of the manuscript".

For the two-level converter modeling it is assumed that: 1) the IGBTs are ideal and unidirectional, and they will never be subject to inverse voltages, being this situation guaranteed by the arrangement of connection in anti-parallel diodes; 2) the diodes are ideal: in conduction it is null the voltage between its terminals, and in blockade it is null the current that passes through it; 3) the voltage in the exit of the rectifier should always be $v_{dc} > 0$ ; 4) each leg $k$ of the converter should always have one IGBT on a conduction state.

For the switching function of each IGBT, the switching variable $\gamma_k$ is used to identify the state of the IGBT $i$ in the leg $k$ of the converter. The index $i$ with $i \in \{1,2\}$ identifies the IGBT. The index $k$ with $k \in \{1,2,3\}$ identifies a leg for the rectifier and $k \in \{4,5,6\}$ identifies the inverter one. The two conditions [11] for the switching variable of each leg $k$ are given by:

$$\gamma_k = \begin{cases} 1, & (S_{1k} = 1 \text{ and } S_{2k} = 0) \\ 0, & (S_{1k} = 0 \text{ and } S_{2k} = 1) \end{cases} \qquad k \in \{1, \ldots, 6\} \tag{17}$$

The topological restriction for the leg $k$ is given by:

$$\sum_{i=1}^{2} S_{ik} = 1 \qquad k \in \{1, \ldots, 6\} \tag{18}$$

Hence, each switching variable depends on the conduction and blockade states of the IGBTs. The phase currents injected in the electric network are modeled by the state equation:

$$\frac{di_k}{dt} = \frac{1}{(L_c + L_f)}(u_{sk} - R_c i_k - u_k) \qquad k = \{4,5,6\} \tag{19}$$

The capacitor voltage $v_{dc}$ is modeled by the state equation:

$$\frac{dv_{dc}}{dt} = \frac{1}{C}\left(\sum_{k=1}^{3} \gamma_k i_k - \sum_{k=4}^{6} \gamma_k i_k\right) \tag{20}$$

Hence, the two-level converter is modeled by (17) to (20).

*2.5 Multilevel converter*

The multilevel converter is an AC-DC-AC converter, with twelve unidirectional commanded IGBTs $S_{ik}$ used as a rectifier, and with the same number of unidirectional commanded IGBTs used as an inverter. The rectifier is connected between the PMSG and a capacitor bank. The inverter is connected between this capacitor bank and a second order filter, which in turn is connected to an electric network.

The groups of four IGBTs linked to the same phase constitute a leg $k$ of the converter. A three-phase active symmetrical circuit in series models the electric network.

The configuration of the simulated WECS with multilevel converter is shown in Fig. 4.

"See Fig. 4 at the end of the manuscript".

For the multilevel converter modeling it is also assumed that: 1) the IGBTs are ideal and unidirectional, and they will never be subject to inverse voltages, being this situation guaranteed by the arrangement of connection in anti-parallel diodes; 2) the diodes are ideal: in conduction it is null the voltage between its terminals and in blockade it is null the current that passes through it; 3) the voltage in the exit of the rectifier should always be $v_{dc} > 0$ ; 4) each leg $k$ of the converter should always have two IGBTs on conduction state.

For the switching function of each IGBT, the switching variable $\gamma_k$ is used to identify the state of the IGBT $i$ in the leg $k$ of the converter. The index $i$ with $i \in \{1,2,3,4\}$ identifies the IGBT. The index $k$ with $k \in \{1,2,3\}$ identifies the leg for the rectifier and $k \in \{4,5,6\}$ identifies the inverter one. The three valid conditions [11] for the switching variable of each leg $k$ are as follows:

$$\gamma_k = \begin{cases} 1, & (S_{1k} \text{ and } S_{2k}) = 1 \quad \text{and} \quad (S_{3k} \text{ or } S_{4k}) = 0 \\ 0, & (S_{2k} \text{ and } S_{3k}) = 1 \quad \text{and} \quad (S_{1k} \text{ or } S_{4k}) = 0 \\ -1, & (S_{3k} \text{ and } S_{4k}) = 1 \quad \text{and} \quad (S_{1k} \text{ or } S_{2k}) = 0 \end{cases} \qquad k \in \{1, \ldots, 6\} \tag{21}$$

The topological restriction for the leg $k$ is given by:

$$(S_{1k}.S_{2k}) + (S_{2k}.S_{3k}) + (S_{3k}.S_{4k}) = 1 \qquad k \in \{1, \ldots, 6\} \tag{22}$$

With the two upper IGBTs in each leg $k$ ($S_{1k}$ and $S_{2k}$) of the converters it is associated a switching variable $\Gamma_{1k}$ and also for the two lower IGBTs ($S_{3k}$ and $S_{4k}$) it is associated a variable $\Gamma_{1k}$, respectively given by:

$$\Gamma_{1k} = \frac{\gamma_k(1+\gamma_k)}{2} \;\; ; \;\; \Gamma_{2k} = \frac{\gamma_k(1-\gamma_k)}{2} \qquad k \in \{1, \ldots, 6\} \tag{23}$$

Hence, each switching variable depends on the conduction and blockade states of the IGBTs. The phase currents injected in the electric network are modeled by the state equation:

$$\frac{di_{fk}}{dt} = \frac{1}{L_c}(u_{fk} - R_c i_{fk} - u_k) \qquad k = \{4,5,6\} \tag{24}$$

The capacitor voltage $v_{dc}$ is the sum of the voltages $v_{C1}$ and $v_{C2}$ in the capacitor banks $C_1$ and $C_2$, modeled by the state equation:

$$\frac{dv_{dc}}{dt} = \frac{1}{C_1}\left(\sum_{k=1}^{3} \Gamma_{1k} i_k - \sum_{k=4}^{6} \Gamma_{1k} i_k\right) + \frac{1}{C_2}\left(\sum_{k=1}^{3} \Gamma_{2k} i_k - \sum_{k=4}^{6} \Gamma_{2k} i_k\right) \tag{25}$$

Hence, the multilevel converter is modeled by (21) to (25).

## 3. Control strategy

Power converters are variable structure systems, because of the on/off switching of their IGBTs. The controllers used in the converters are PI controllers. PWM by SVM associated with sliding mode control is used for controlling the converters.

The sliding mode control strategy presents attractive features such as robustness to parametric uncertainties of the turbine and the generator as well as to electric grid disturbances [37].

Sliding mode control is particularly interesting in systems with variable structure, such as switching power converters, guaranteeing the choice of the most appropriate space vectors. The aim is to let the system slide along a predefined sliding surface by changing the system structure.

The power semiconductors have physical limitations to be considered during design phase and during simulation. Particularly, they cannot switch at infinite frequency. Also, for a finite value of the switching frequency, an error $e_{\alpha\beta}$ will exist between the reference value and the control value. In order to guarantee that the system slides along the sliding surface $S(e_{\alpha\beta},t)$, it has been proven that it is necessary to ensure that the state trajectory near the surfaces verifies the stability conditions [10,11] given by:

$$S(e_{\alpha\beta},t)\ \frac{dS(e_{\alpha\beta},t)}{dt} < 0 \tag{26}$$

in practice a small error $\varepsilon > 0$ for $S(e_{\alpha\beta},t)$ is allowed, due to power semiconductors switching only at finite frequency.

Consequently, a switching strategy has to be considered, given by:

$$-\varepsilon < S(e_{\alpha\beta},t) < +\varepsilon \tag{27}$$

At the simulation level, a practical implementation of the switching strategy considered in (27) could be accomplished by using hysteresis comparators.

The output voltages of matrix converter are switched discontinuous variables. If high enough switching frequencies are considered (much higher than the input and output matrix converter fundamental frequencies), it is possible to assume that in each switching period $T_s$, the average value of the output voltages is nearly equal to their reference average value. Hence, the equality is given by:

$$\frac{1}{T_s}\int_{nT_s}^{(n+1)T_s} v_{\alpha\beta}\, dt = v_{\alpha\beta}^{*} \tag{28}$$

Similar to output voltages, the input current average value is nearly equal to their reference average value. Hence, the equality is given by:

$$\frac{1}{T_s}\int_{nT_s}^{(n+1)T_s} i_q\, dt = i_q^{*} \tag{29}$$

The output voltage vectors and the input current vectors in the $\alpha\beta$ plane for the matrix converter are shown in Fig. 5 and Fig. 6, respectively.

"See Fig. 5 at the end of the manuscript".

"See Fig. 6 at the end of the manuscript".

The outputs of the hysteresis comparators are integer variables [10]. The voltage integer variables $\sigma_{\alpha\beta}$ for the matrix converter take the values:

$$\sigma_{\alpha\beta} \quad \text{with} \quad \sigma_\alpha, \sigma_\beta \in \{-1, 0, 1\} \tag{30}$$

The current integer variables $\sigma_q$ for the matrix converter in $dq$ coordinates take the values:

$$\sigma_q \in \{-1, 1\} \tag{31}$$

The appropriate vector selection in order to ensure stability for the matrix converter is shown in Table 1.

"See Table 1 at the end of the manuscript".

where $\Phi_u$ represent the input voltage instantaneous phase.

The output voltage vectors in the $\alpha\beta$ plane for the two-level converter are shown in Fig. 7.

"See Fig. 7 at the end of the manuscript".

Also, the integer variables $\sigma_{\alpha\beta}$ for the two-level converter take the values:

$$\sigma_{\alpha\beta} \quad \text{with} \quad \sigma_\alpha, \sigma_\beta \in \{-1, 0, 1\} \tag{32}$$

The appropriate vector selection in order to ensure stability for the two-level converter is shown in Table 2.

"See Table 2 at the end of the manuscript".

The output voltage vectors in the $\alpha\beta$ plane for the multilevel converter are shown in Fig. 8.

"See Fig. 8 at the end of the manuscript".

The integer variables $\sigma_{\alpha\beta}$ for the multilevel converter take the values:

$$\sigma_{\alpha\beta} \quad \text{with} \quad \sigma_\alpha, \sigma_\beta \in \{-2,-1,0,1,2\} \tag{33}$$

If $u_{C1} \neq u_{C2}$, then a new vector is selected. The appropriate vector selection in order to ensure stability for the multilevel converter is shown in Table 3, for $u_{C1} > u_{C2}$, and in Table 4, for $u_{C1} < u_{C2}$.

"See Table 3 at the end of the manuscript".

"See Table 4 at the end of the manuscript".

Hence, the proposed control strategy for the power converters is given by (26) to (33).

**4. Design of power coefficient**

The choice of the wind turbines is dependent on the prospective site where the wind turbine is located. The prospective site is an important issue that should be considered for the success of the implementation. The wind speed highly influences the mechanical power acquired by a WECS. Even a small variation in the absolute value of the wind speed may result in a significant change on the mechanical power, due to the cubic relationship between velocity and power. Hence, the behavior of the wind at a prospective site should be properly analyzed and understood. Realizing the nature of wind is important for an appropriate design, which allows adequate tuning with the wind characteristics expected at this prospective site [38].

The identification of the wind variability at a site is often achieved by grouping the data, using a frequency distribution probability function, usually a Weibull or a Rayleight distribution. Suppose a variable-speed horizontal axis WECS is installed, with three blades, upwind at a site with the wind data given by the frequency distribution shown in Fig. 9.

"See Fig. 9 at the end of the manuscript".

The average wind speed is $v_m = 8.2\ m/s$ for the distribution given in Fig. 9. The wind turbine will be in operation most of the time for wind speeds ranging between 5 m/s and 10 m/s. The rotor speed varies smoothly during the accumulation of kinetic energy in the rotor [12]. When rated wind turbine speed is reached, if a sudden wind gust appears the rotor speed is allowed to increase until 10%. This is due to the fact that the pitch control response is not instantaneous. Hence, it cannot respond in due time to sudden wind gusts.

The stored kinetic energy can be employed to further smooth fluctuations in the available wind power [31]. The wind turbine has rated wind speed of 13 m/s, maintaining energy conversion for wind speeds until 25 m/s. The wind turbine works with tip speeds between 25.65 m/s, for the cut-in wind speed of 2.5 m/s, and 81.04 m/s, between the wind speed of 16 m/s and the cut-out wind speed of 25 m/s. Hence, the power coefficient is designed as a function of the wind speed, as shown in Fig. 10.

"See Fig. 10 at the end of the manuscript".

The power coefficient increases until 8 m/s, and between 8 m/s and 10 m/s the power coefficient is constant at the maximum power coefficient. At wind speeds greater than 10 m/s the power coefficient is decreased and at wind speeds greater than 13 m/s the power is maintained at its rated value.

**5. Simulation results**

The mathematical models for the WECS with the matrix, two-level and multilevel power converter topologies were implemented in Matlab/Simulink. The WECS simulated in this case study has a rated electric power of 900 kW. A wind speed upstream of the rotor given by a ramp increase is considered in the simulation, taking 2.5 s between the speeds of 4.5 m/s and 25 m/s. Also, a time horizon of 3.5 s is considered. The switching frequency for the IGBTs is 5 kHz.

Fig. 11 shows blades pitch angle variation with the wind speed.

"See Fig. 11 at the end of the manuscript".

Thus, the pitch angle varies with the wind speed, between 13 m/s and 25 m/s, in order to avoid over-rated power excursion of the WECS. But, between 16 m/s and 25 m/s the pitch angle varies in order not only to avoid over-rated power excursion, but also to maintain the tip speed at 81.04 m/s.

The mechanical power of the wind turbine $P_t$, the electric power of the generator $P_g$, and the difference between these two powers, i.e., the accelerating power, are shown in Fig. 12.

"See Fig. 12 at the end of the manuscript".

The next two figures show simulation results for the WECS with the matrix converter. The instantaneous three-phase currents injected in the grid are shown in Fig. 13.

"See Fig. 13 at the end of the manuscript".

The root mean square (RMS) current injected in the grid is shown in Fig. 14.

"See Fig. 14 at the end of the manuscript".

The next three figures show simulation results for the WECS with the two-level converter. The capacitor voltage $v_{dc}$ is shown in Fig. 15.

"See Fig. 15 at the end of the manuscript".

The instantaneous three-phase currents injected in the grid are shown in Fig. 16.

"See Fig. 16 at the end of the manuscript".

The RMS current injected in the grid is shown in Fig. 17.

"See Fig. 17 at the end of the manuscript".

The next three figures show simulation results for the WECS with the multilevel converter. The capacitor voltage $v_{dc}$ is the sum of the voltages $v_{C1}$ and $v_{C2}$, respectively at the capacitor banks $C_1$ and $C_2$. These voltages are shown in Fig. 18.

"See Fig. 18 at the end of the manuscript".

The instantaneous three-phase currents injected in the grid are shown in Fig. 19.

"See Fig. 19 at the end of the manuscript".

The RMS current injected in the grid is shown in Fig. 20.

"See Fig. 20 at the end of the manuscript".

Fig. 18 shows that the capacitors voltages $v_{C1}$ and $v_{C2}$ are nearly equal, and approximately half of the $v_{dc}$ voltage, which is of the utmost importance for the multilevel converter since an unbalance may result in a malfunction on the control. Also, it is important to notice that the voltages across the IGBTs of the two-level converter, Fig. 15, are greater than those of the multilevel converter, Fig. 18. This is an advantage for the multilevel converter.

The presence of the energy-storage elements, in comparison with the matrix converter, and the increasing number of voltage levels together with the consideration of a second order filter, in comparison with the two-level converter, allows the WECS with the multilevel converter to achieve the best performance: higher power quality waveforms (Fig. 19 and Fig. 20).

## 6. Conclusions

The increased wind power penetration leads to new technical challenges, implying research for more realistic physical models of WECSs. The paper presents a new integrated model for WECSs, considering a more accurate dynamic of the variable-speed wind turbine, having a two-mass model drive train, a PMSG, and three different topologies for the power-electronic converters: matrix, two-level and multilevel. The control strategy is based on PWM by SVM associated with sliding mode control, and power factor control is introduced at the output of the power converters. Although more complex, this control strategy is justified for more realistic results. The two-mass model for the rotor is relevant in oscillatory studies for the prediction of the WECS behavior. Simulation results have shown that the best performance of the WECS, regarding power quality, is achieved with the use of multilevel converters.

## References

[1] Peças Lopes J, Hatziargyriou N, Mutale J, Djapic P, Jenkins N. Integrating distributed generation into electric power systems: a review of drivers, challenges and opportunities. Electric Power Systems Research 2007; 77 (9): 1189-1203.

[2] Blaabjerg F, Chen Z, Kjaer SB. Power electronics as efficient interface in dispersed power generation systems. IEEE Transactions Industrial Electronics 2004; 19 (5): 1184-1194.

[3] Blaabjerg F, Teodoresco R, Liserre M, Timbus AV. Overview of control and grid synchronization for distributed power generation systems. IEEE Trans. Ind. Electron. 2006; 53 (5): 1398-1409.

[4] Catalão JPS, Mariano SJPS, Mendes VMF, Ferreira LAFM. Short-term scheduling of thermal units: emission constraints and trade-off curves. Eur. Trans. Electr. Power 2008; 18 (1): 1-14.

[5] Estanqueiro A, Castro R, Flores P, Ricardo J, Pinto M, Rodrigues R, Peças Lopes J. How to prepare a power system for 15% wind energy penetration: the Portuguese case study. Wind Energy 2008; 3 (3): 75-84.

[6] Erlich I, Kretschmann J, Fortmann J, Mueller-Engelhardt S, Wrede H. Modelling of wind turbines based on doubly-fed induction generators for power system stability studies. IEEE Trans. Power Syst. 2007; 22 (3): 909-919.

[7] Almeida RG, Peças Lopes JA. Participation of doubly fed induction wind generators in system frequency regulation. IEEE Trans. Power Syst. 2007; 22 (3): 944-950.

[8] Carrasco JM, Franquelo LG, Bialasiewicz JT, Galvan E, Guisado RCP, Prats AM, Leon JI, Moreno-Alfonso N. Power-electronic systems for the grid integration of renewable energy sources: A survey. IEEE Trans. Ind. Electron. 2006; 53 (4): 1002-1016.

[9] Estanqueiro AI. A dynamic wind generation model for power systems studies. IEEE Trans. Power Syst. 2007; 22 (3): 920-928.

[10] Melício R, Mendes VMF, Catalão JPS. Modeling and simulation of a wind energy system: matrix versus multilevel converters. In: Proc. 14th IEEE Mediterr. Electrotechnical Conf., Ajaccio, France 2008; 604-609.

[11] Melício R, Mendes VMF, Catalão JPS. Two-level and multilevel converters for wind energy systems: a comparative study. In: Proc. 13th Int. Power Electron. Motion Control Conf., Poznań, Poland, 2008; 1682-1687.

[12] Baroudi JA, Dinavahi V, Knight AM. A review of power converter topologies for wind generators. Renewable Energy 2007; 32 (14): 2369-2385.

[13] Gaillard A, Poure P, Saadate S, Machmoumc M. Variable speed DFIG wind energy system for power generation and harmonic current mitigation. Renewable Energy 2009; 34 (6): 1545-1553.

[14] Fernandez LM, Garcia CA, Jurado F. Operating capability as a PQ/PV node of a direct-drive wind turbine based on a permanent magnet synchronous generator. Renewable Energy 2010; 35 (6): 1308-1318.

[15] Ramtharan G, Jenkins N, Anaya-Lara O, Bossanyi E. Influence of rotor structural dynamics representations on the electrical transient performance of FSIG and DFIG wind turbines. Wind Energy 2007; 10: 293-301.

[16] Li H, Chen Z. Design optimization and site matching of direct-drive permanent magnet wind power generator systems. Renewable Energy 2009; 34 (4): 1175-1184.

[17] Henschel M, Hartkopf T, Schneider H, Troester E. A reliable and efficient new generator system for offshore wind farms with DC farm grid. In: Proc. IEEE 33rd Annu. Power Electron. Spec. Conf., Cairns, Australia 2002; 111-116.

[18] Conroy JF, Watson R. Low-voltage ride-through of a full converter wind turbine with permanent magnet generator. IET Renew. Power Gener. 2007; 1 (3): 182-189.

[19] Sánchez JA, Veganzones C, Martinez S, Blazquez F, Herrero N, Wilhelmi JR. Dynamic model of wind energy conversion systems with variable speed synchronous generator and full-size power converter for large-scale power system stability studies. Renewable Energy 2008; 33 (6): 1186-1198.

[20] Wheeler PW, Rodriguez J, Clare JC, Empringham L, Weinstein A. Matrix converters: A technology review. IEEE Trans. Ind. Electron. 2002; 49 (2): 276-288.

[21] Cardenas R, Peña R, Wheeler P, Clare J. Reactive power capability of WECS based on matrix converter. Electron. Lett. 2008; 44 (11): 674-676.

[22] Jia S, Wang X, Tseng KJ. Matrix converters for wind energy systems. In: IEEE Conf. Ind. Electron. Appl. 2007; 488-494.

[23] Lai JS, Peng FZ. Multilevel converters—A new breed of power converters. IEEE Trans. Ind. Appl. 1996; 32 (3): 509-517.

[24] Portillo RC, Prats MM, Leon JI, Sanchez JA, Carrasco JM, Galvan E, Franquelo LG. Modeling strategy for back-to-back three-level converters applied to high-power wind turbines. IEEE Trans. Ind. Electron. 2006; 53 (5): 1483-1491.

[25] Abbes M, Belhadj J, Bennani ABA. Design and control of a direct drive wind turbine equipped with multilevel converters. Renewable Energy 2010; 35 (5): 936-945.

[26] Rodriguez J, Lai J-S, Peng FZ. Multilevel inverters: A survey of topologies, controls, and applications. IEEE Trans. Ind. Electron. 2002; 49 (4): 724-738.

[27] Babaei E, Hosseini S H, Gharehpetian G B, Haque MT, Sabahi M. Reduction of dc voltage sources and switches in asymmetrical multilevel converters using a novel topology. Electr. Power Syst. Res. 2007; 77 (8): 1073-1085.

[28] Alepuz S, Busquets-Monge S, Bordonau J, Gago J, Gonzalez D, Balcells J. Interfacing renewable energy sources to the utility grid using a three-level inverter. IEEE Trans. Ind. Electron. 2006; 53 (5): 1504-1511.

[29] Eloy-Garcia J, Arnaltes S, Rodrigez-Amenedo JL. Extended direct power control for multilevel inverters including dc link middle point voltage control. IET Electr. Power Appl. 2007; 1 (4): 571-580.

[30] Rawn BG, Lehn PW, Maggiore M. Control methodology to mitigate the grid impact of wind turbines. IEEE Trans. Energy Convers. 2007; 22 (2): 431-438.

[31] Slootweg JG, de Haan SWH, Polinder H, Kling WL. General model for representing variable speed wind turbines in power system dynamics simulations. IEEE Trans. Power Syst. 2003; 18 (1): 144-151.

[32] Poller MA. Doubly-fed induction machine models for stability assessment of wind farms. In: Proc. IEEE Bologna Power Tech Conf. 2003; Bologna, Italy.

[33] Ong CM. Dynamic simulation of electric machinery. Upper Saddle River: Prentice-Hall; 1998; 259-350.

[34] Senjyu T, Tamaki S, Urasaki N, Uezato K. Wind velocity and position sensorless operation for PMSG wind generator. In: Proc. 5th Int. Conf. on Power Electronics and Drive Systems, Singapore, 2003, pp. 787-792.

[35] Watanabe EH, Stephan RM, Aredes M. New concepts of instantaneous active and reactive powers in electrical systems with generic loads. IEEE Trans. Power Deliv. 1993; 8 (2): 697-703.

[36] Barakati SM, Aplevich JD, Kazerani M. Controller design for a wind turbine system including a matrix converter. In: IEEE Power Eng. Soc. Gen. Meeting 2007, Tampa, FL; 1-8.

[37] Beltran B, Ahmed-Ali T, Benbouzid MEH. Sliding mode power control of variable-speed wind energy conversion systems. IEEE Trans. Energy Convers. 2008; 23 (2); 551-558.

[38] Mathew S. Wind energy, fundamentals, resource analysis and economics. Berlin: Springer-Verlag; 2006.

**Figure captions**

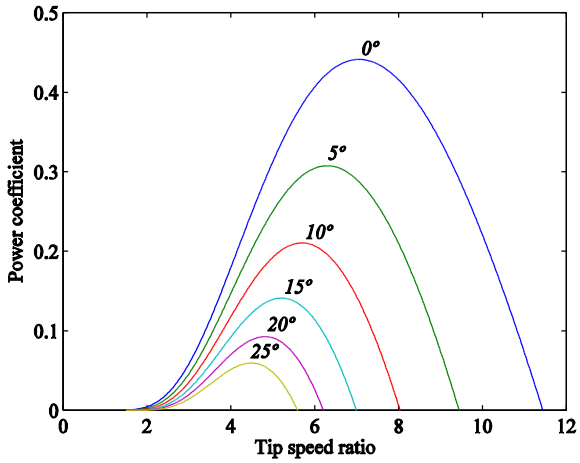


Fig. 1. Power coefficient as a function of the tip speed ratio, parameterized in function of the pitch angle.

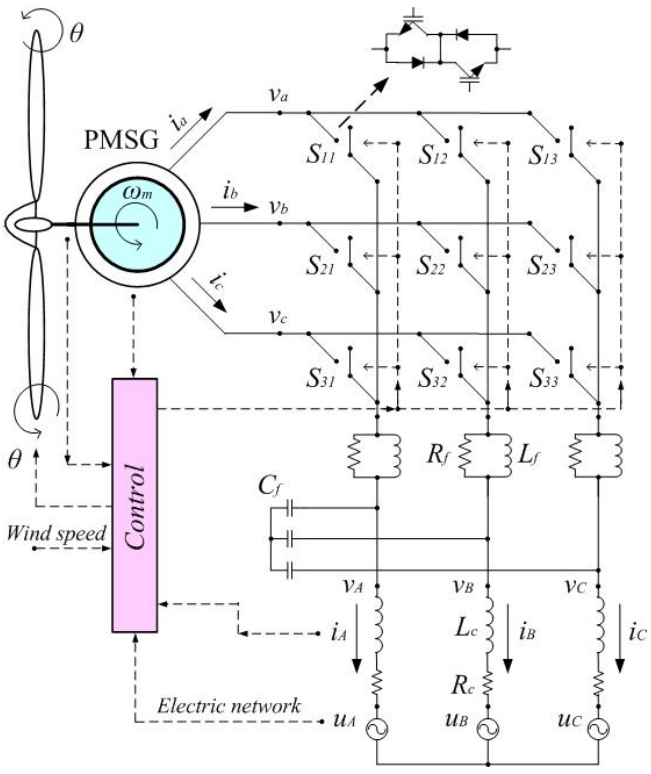


Fig. 2. The simulated WECS with matrix converter.

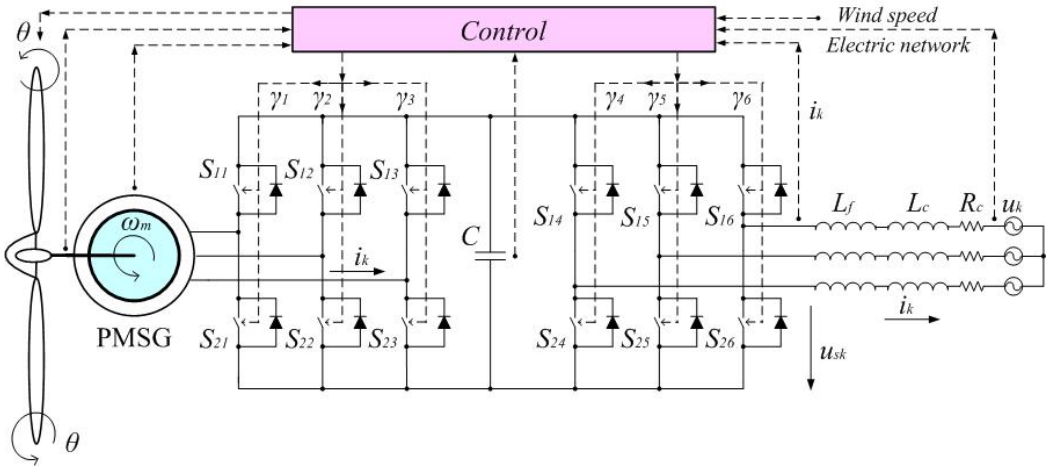


Fig. 3. The simulated WECS with two-level converter.

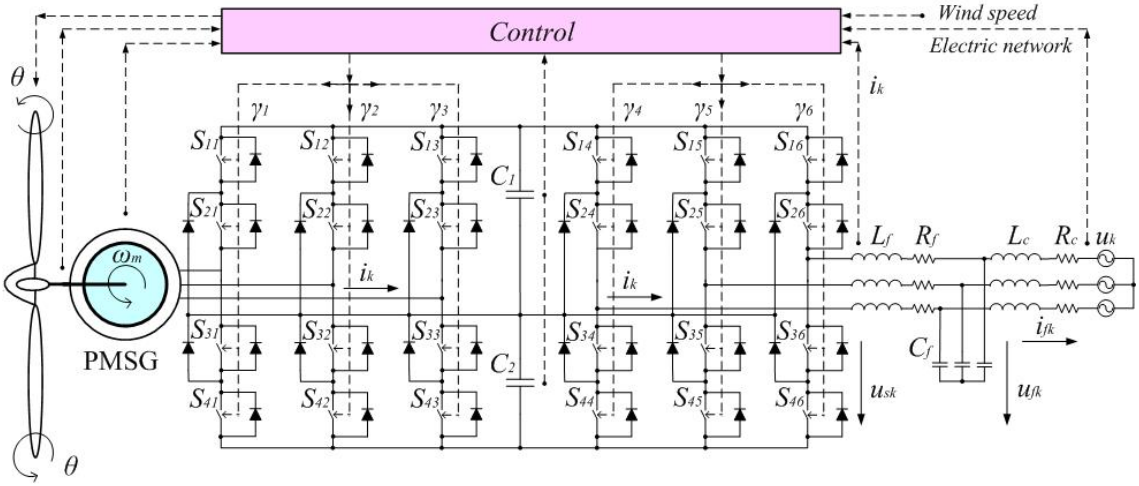


Fig. 4. The simulated WECS with multilevel converter.

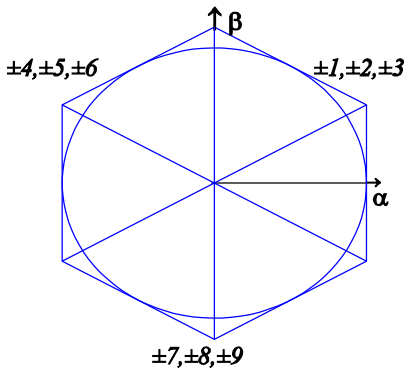


Fig. 5. Output voltage vectors for the matrix converter.

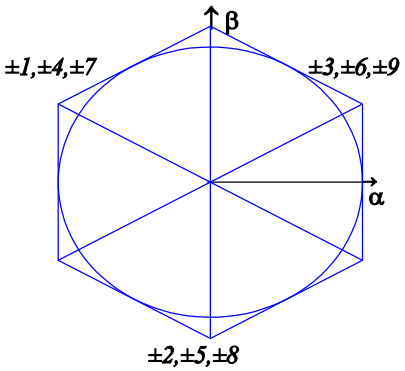


Fig. 6. Input current vectors for the matrix converter.

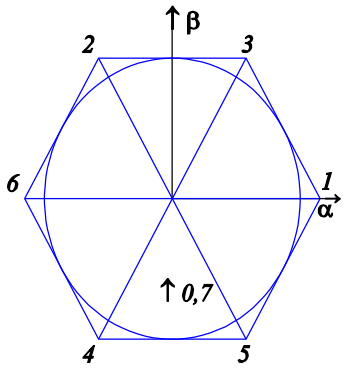


Fig. 7. Output voltage vectors for the two-level converter.

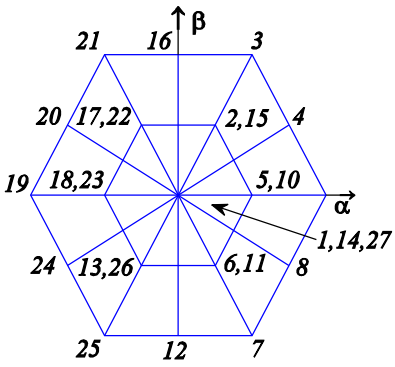


Fig. 8. Output voltage vectors for the multilevel converter.

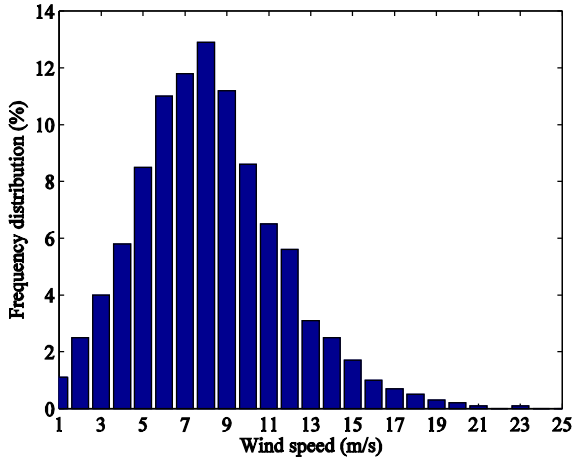


Fig. 9. Wind speed frequency distribution curve.

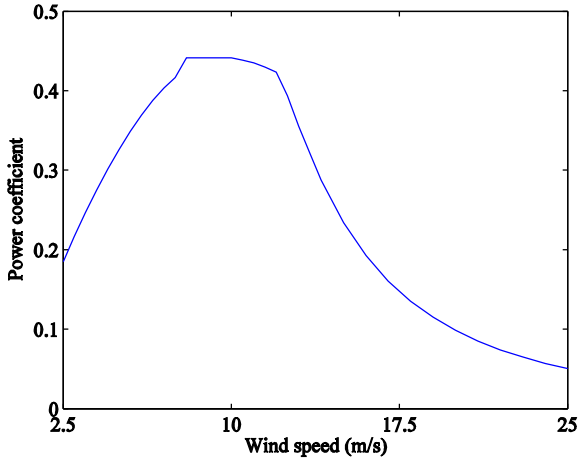


Fig. 10. Power coefficient versus wind speed.

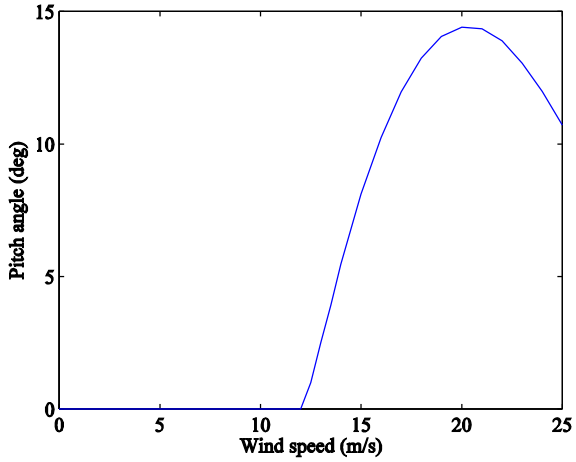


Fig. 11. Pitch angle in function of wind speed.

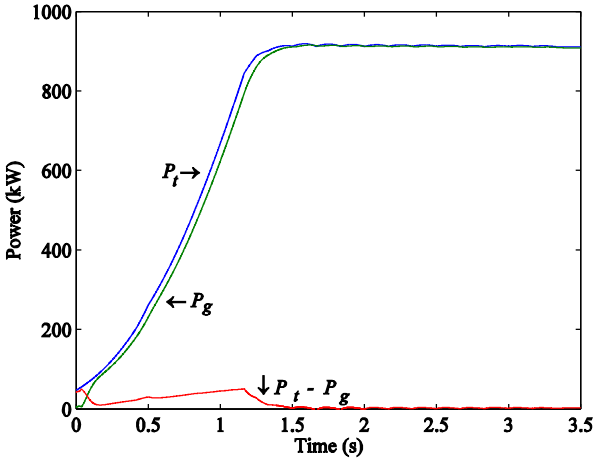


Fig. 12. Mechanical, electric and accelerating power.

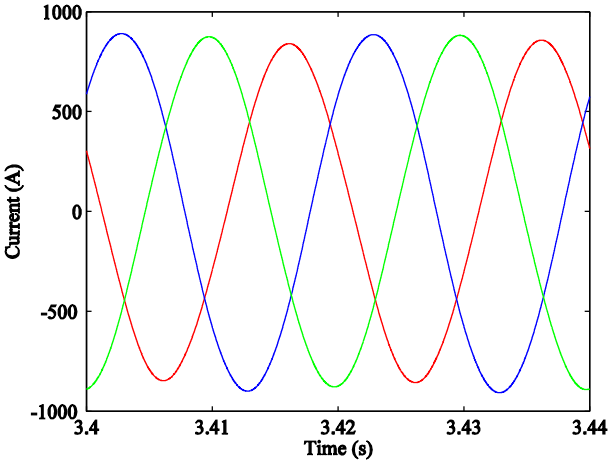


Fig. 13. Output current for the matrix converter.

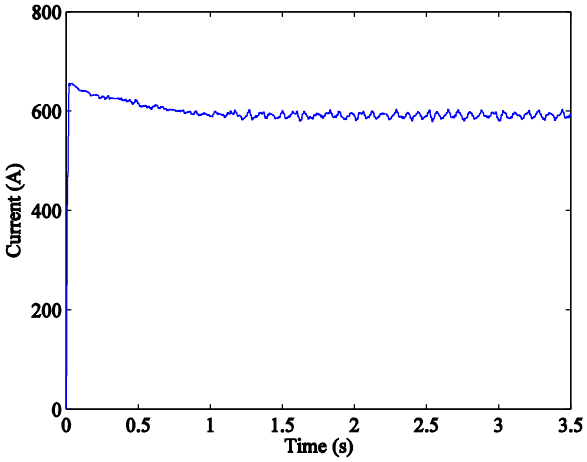


Fig. 14. Output RMS current for the matrix converter.

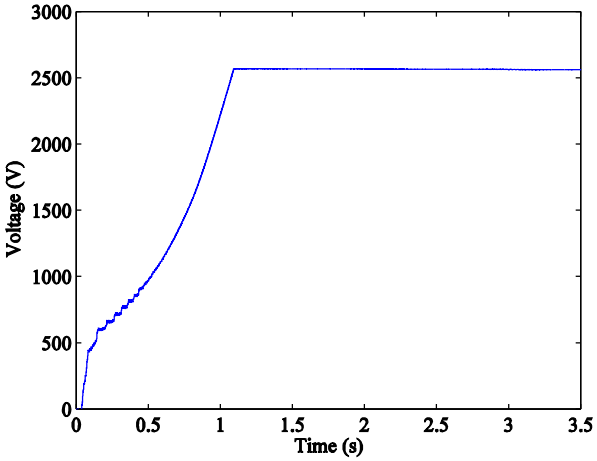


Fig. 15. Capacitor voltage for the two-level converter.

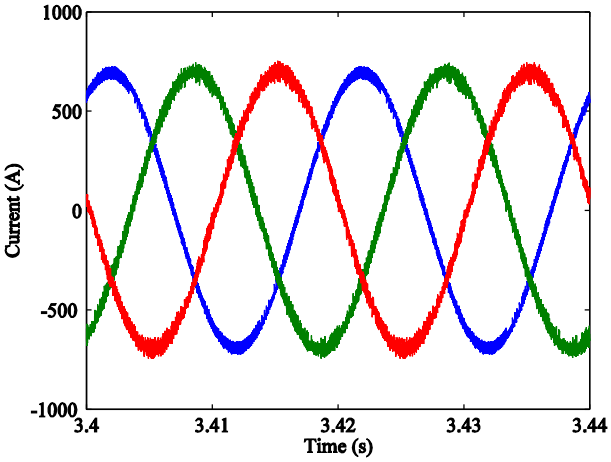


Fig. 16. Output current for the two-level converter.

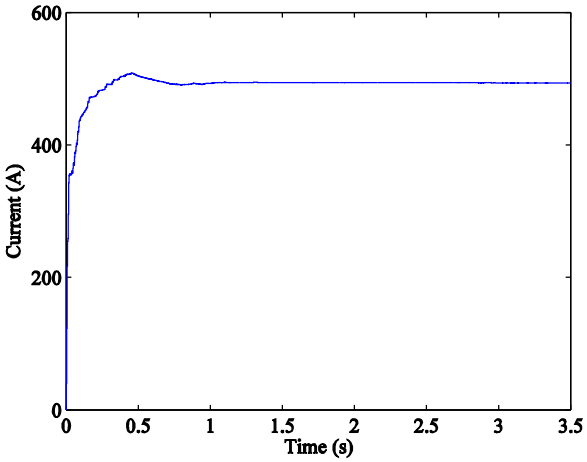


Fig. 17. Output RMS current for the two-level converter.

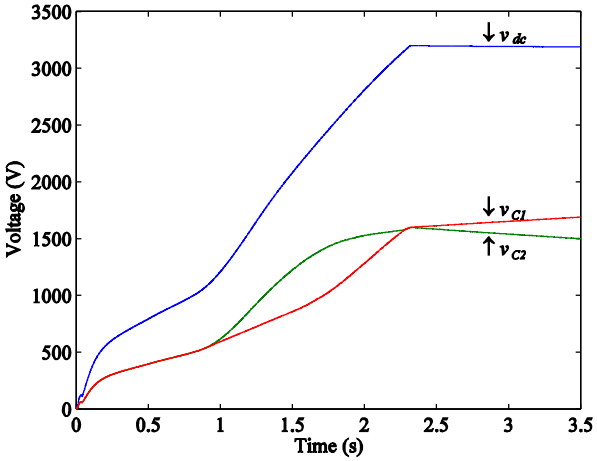


Fig. 18. Capacitors voltages for the multilevel converter.

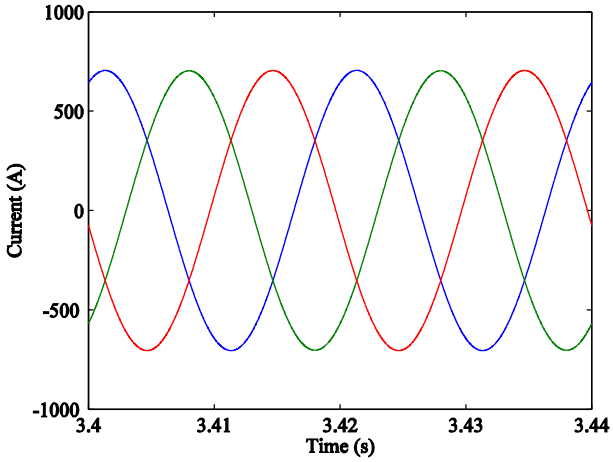


Fig. 19. Output current for the multilevel converter.

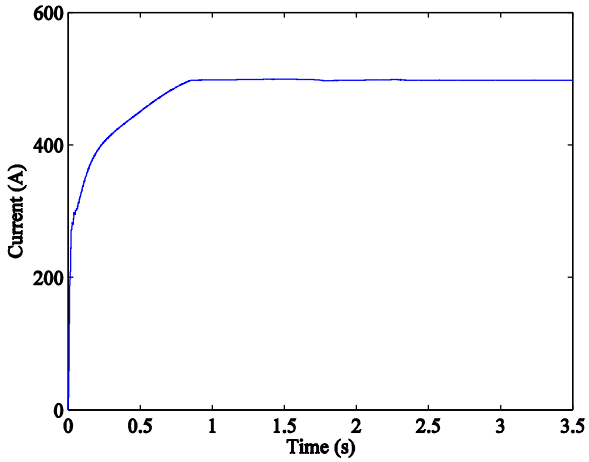


Fig. 20. Output RMS current for the multilevel converter.

## Tables

Table 1
Output voltage and input current vectors selection for the matrix converter

| Voltage switching strategy | | Input voltage instantaneous phase | | | | | | | | | | | |
|---|---|---|---|---|---|---|---|---|---|---|---|---|---|
| | | $11\pi/6 \le \Phi_u < \pi/6$ | | $\pi/6 \le \Phi_u < \pi/2$ | | $\pi/2 \le \Phi_u < 5\pi/6$ | | $5\pi/6 \le \Phi_u < 7\pi/6$ | | $7\pi/6 \le \Phi_u < 3\pi/2$ | | $3\pi/2 \le \Phi_u < 11\pi/6$ | |
| $\sigma_\alpha$ | $\sigma_\beta$ | $\sigma_q$ Current switching strategy | | | | | | | | | | | |
| | | **-1** | **1** | **-1** | **1** | **-1** | **1** | **-1** | **1** | **-1** | **1** | **-1** | **1** |
| **-1** | **-1** | -2 | +3 | -2 | +3 | +3 | -2 | +3 | -2 | +3 | -2 | -2 | +3 |
| **-1** | **0** | -2 | +3 | -2 | +3 | +3 | -2 | +3 | -2 | +3 | -2 | -2 | +3 |
| **-1** | **1** | +5 | -6 | -6 | +5 | -6 | +5 | -6 | +5 | +5 | -6 | +5 | -6 |
| **0** | **-1** | +8 | -9 | +8 | -9 | +8 | -9 | -9 | +8 | -9 | +8 | -9 | +8 |
| **0** | **0** | 0 | 0 | 0 | 0 | 0 | 0 | 0 | 0 | 0 | 0 | 0 | 0 |
| **0** | **1** | +9 | -8 | +9 | -8 | +9 | -8 | -8 | +9 | -8 | +9 | -8 | +9 |
| **1** | **-1** | +6 | -5 | -5 | +6 | -5 | +6 | -5 | +6 | +6 | -5 | +6 | -5 |
| **1** | **0** | -3 | +2 | -3 | +2 | +2 | -3 | +2 | -3 | +2 | -3 | -3 | +2 |
| **1** | **1** | -3 | +2 | -3 | +2 | +2 | -3 | +2 | -3 | +2 | -3 | -3 | +2 |

Table 2
Output voltage vectors selection for the two-level converter

| $\sigma_\beta \setminus \sigma_\alpha$ | **-1** | **0** | **1** |
|---|---|---|---|
| **-1** | 4 | 4;5 | 5 |
| **0** | 6 | 0;7 | 1 |
| **1** | 2 | 3;2 | 3 |

Table 3
Output voltage vectors selection for the multilevel converter, for $u_{C1} > u_{C2}$

| $\sigma_\beta \setminus \sigma_\alpha$ | **-2** | **-1** | **0** | **1** | **2** |
|---|---|---|---|---|---|
| **-2** | 25 | 25 | 12 | 7 | 7 |
| **-1** | 24 | 13 | 13;6 | 6 | 8 |
| **0** | 19 | 18 | 1;14;27 | 5 | 9 |
| **1** | 20 | 17 | 17;2 | 2 | 4 |
| **2** | 21 | 21 | 16 | 3 | 3 |

Table 4
Output voltage vectors selection for the multilevel converter, for $u_{C1} < u_{C2}$

| $\sigma_\beta \setminus \sigma_\alpha$ | **-2** | **-1** | **0** | **1** | **2** |
|---|---|---|---|---|---|
| **-2** | 25 | 25 | 12 | 7 | 7 |
| **-1** | 24 | 26 | 26;11 | 11 | 8 |
| **0** | 19 | 23 | 1;14;27 | 10 | 9 |
| **1** | 20 | 22 | 22;15 | 15 | 4 |
| **2** | 21 | 21 | 16 | 3 | 3 |